PNL-6362
UC-70

2F

Nuclear Waste Treatment Program

Evaluation of Liquid-Fed Ceramic Melter Scale-Up Correlations

S. S. Koegler
S. J. Mitchell

August 1988

Prepared for the U.S. Department of Energy
under Contract DE-AC06-76RLO 1830

Pacific Northwest Laboratory
Operated for the U.S. Department of Energy
by Battelle Memorial Institute

Battelle

PNL-6362

DISCLAIMER

PACIFIC NORTHWEST LABORATORY
operated by
BATTELLE MEMORIAL INSTITUTE
for the
UNITED STATES DEPARTMENT OF ENERGY
under Contract DE-AC06-76RLO 1830

Printed in the United States of America
Available from
National Technical Information Service
United States Department of Commerce
5285 Port Royal Road
Springfield, Virginia 22161

NTIS Price Codes
Microfiche A01

Printed Copy

Pages	Price Codes
001-025	A02
026-050	A03
051-075	A04
076-100	A05
101-125	A06
126-150	A07
151-175	A08
176-200	A09
201-225	A10
226-250	A11
251-275	A12
276-300	A13

PNL-6362
UC-70

NUCLEAR WASTE TREATMENT PROGRAM

EVALUATION OF LIQUID-FED CERAMIC MELTER SCALE-UP CORRELATIONS

S. S. Koegler
S. J. Mitchell

August 1988

Prepared for
the U.S. Department of Energy
under Contract DE-AC06-76RLO 1830

Pacific Northwest Laboratory
Richland, Washington 99352

SUMMARY

This study was conducted to determine the parameters governing factors of scale for liquid-fed ceramic melters (LFCMs) in order to design full-scale melters using smaller-scale melter data. Results of melter experiments conducted at Pacific Northwest Laboratory (PNL) and Savannah River Laboratory (SRL) are presented for two feed compositions and five different liquid-fed ceramic melters. The melter performance data including nominal feed rate and glass melt rate are correlated as a function of melter surface area. Comparisons are made between the actual melt rate data and melt rates predicted by a cold cap heat transfer model. The heat transfer model could be used in scale-up calculations, but insufficient data are available on the cold cap characteristics. Experiments specifically designed to determine heat transfer parameters are needed to further develop the model.

CONTENTS

SUMMARY iii

INTRODUCTION 1

PRIOR MELTER MODELING WORK 3

GENERAL PROCESSING CONSIDERATIONS 3

COMMERCIAL GLASS MELTER SCALE-UP 4

THEORETICAL/NUMERICAL MODELS 4

PHYSICAL MODELS 5

COLD CAP HEAT TRANSFER MODEL 7

EXPERIMENTAL WORK 9

CORRELATION OF RESULTS 13

SCALE-UP BY MELTER SURFACE AREA 13

SCALE-UP BY COLD CAP HEAT TRANSFER 16

CONCLUSIONS AND RECOMMENDATIONS 21

REFERENCES 23

APPENDIX A - EXPERIMENTAL WORK DETAILS A.1

APPENDIX B - ROUTT MODEL CALCULATIONS B.1

APPENDIX C - CALCULATION OF BOUNDARY-LAYER THICKNESS C.1

FIGURES

1 Nominal Slurry Feed Rate 13

2 Nominal Glass Melt Rate 14

3 Feed Rate Versus Surface Area 16

4 Melt Rate Versus Surface Area 16

5 Actual and Calculated Glass Melt Rate for SRL-TDSF-131 Feed (V = 0.25 cm/s) 17

6 Actual and Calculated Glass Melt Rate for HWVP Feed with Sugar (V = 0.25 cm/s) 18

7 Actual and Calculated Glass Melt Rate for HWVP Feed Without Sugar (V = 0.25 cm/s) 18

8 Actual and Calculated Glass Melt Rate for SRL-TDSF-131 Feed (V = 10 cm/s) 19

9 Actual and Calculated Glass Melt Rate for HWVP Feed with Sugar (V = 10 cm/s) 19

10 Actual and Calculated Glass Melt Rate for HWVP Feed Without Sugar (V = 10 cm/s) 20

TABLES

1 Melter Characteristics 9

2 Summary of Experimental Data 10

3 Melter Scale-Up Calculations 15

INTRODUCTION

The joule-heated liquid-fed ceramic melter (LFCM) was developed to immobilize high-level radioactive wastes (HLW) prior to final disposal. The HLW slurry is combined with glass-forming chemicals and melted at a high temperature to produce a stable glass that is highly resistant to attack by groundwater. The LFCM is the product of many years of waste treatment process development, starting with batch in-can melting in the early 1960s. The LFCM is considered the reference method for fixation of HLW in the United States and several other countries.

Production-scale vitrification plants using LFCM technology are under construction at the U.S. Department of Energy (DOE) Savannah River Plant in South Carolina and at West Valley in New York. Design of the Hanford Waste Vitrification Plant at the Hanford Site is also under way. Several pilot- and engineering-scale units have been operated to support LFCM technology development at the Pacific Northwest Laboratory (PNL),[a] Savannah River Laboratory (SRL), and in other parts of the world. The design of a full-size melter requires a knowledge of parameters governing scale-up so that data from a smaller-scale system can be used.

The goal of this study is to provide insight into the important relationships that control processing throughput. The data from two different glass formulations run in five different-scale melters ranging from laboratory- to pilot-scale are compared with predictions from melter models. The objective of this report is to evaluate the techniques currently available for melter scale-up with respect to melter processing rates. Although important, the effects of melter scale on product quality were not considered.

(a) Operated for DOE by Battelle Memorial Institute.

PRIOR MELTER MODELING WORK

Considerable effort has been devoted to slurry-fed, joule-heated ceramic melter scale-up in several areas including rules of thumb and criteria for glass-furnace design based on surface area and volume and through theoretical and physical models. The melter tank convection patterns, electric potential, and temperature distribution have been studied using small-scale physical models and theoretical/numerical models. Theoretical models have also been applied to the heat transfer conditions in and around the cold cap.

GENERAL PROCESSING CONSIDERATIONS

Weisenburger (1983) described the many factors influencing melter performance. Since the heat flux from the melt provides the energy for the waste conversion, Weisenburger suggests that the melt surface area determines the melt rate capacity. The qualitative cold cap model described in his paper consisted of four zones: 1) boiling, 2) drying, 3) calcination, and 4) glassification. The main heat flux travels through the zones in series. Weisenburger concluded that the largest heat duty is in evaporation. Zone thicknesses change in response to the convective heat transfer in the melt and to the kinetics in the reaction zone.

Other parameters also affect the glass melt rate. Plodinec et al. (1983) noted that melt rate follows solids loading in the feed (from 30% to 60%) and that water removal was constant. Too high a feed rate resulted in melter flooding and in operational and off-gas instability. Bjorklund and Brouns (1983) postulated that higher temperatures toward the top of the glass melt gave more stable operation and provided better heat transfer to the cold cap. Experimental melter work at PNL showed that processing rate is strongly affected by convection. Glass melting rate was increased by a factor of 2.4 in the PNL experimental ceramic melter (ECM) by introducing air bubbles into the melter tank (Bjorklund et al. 1983). For homogenization of the melter glass, good convective mixing is required, which is dependent on temperature gradients in the glass and on glass viscosity. However, convection increases corrosion of the ceramic walls.

COMMERCIAL GLASS MELTER SCALE-UP

The expected output for small (less than 20 tonne/day) electric furnaces melting colored glass is about 1000 kg/m^2 of surface area per day or 1250 kg/m^3 of melter volume per day (Stanek 1977). For clear glasses, the expected output increases to 1500 kg/m^2 per day because of the increased infrared transmission through the glass. Flame-fired furnaces are usually scaled by surface area because heat is transmitted through the glass surface; electric furnaces, by volume because heat is evolved throughout the glass by joule heating. In either case, radiant heat transfer from the melter walls to the body of the glass is important.

This situation is somewhat different for the slurry-fed melter that has a feed pile or cold cap of liquid and solid material covering most of the glass surface. Little radiant heat penetrates the volume of the glass, and heat travels through the glass to the cold cap by convection. There is some radiant heat transfer from the exposed walls to the cold cap, but much of this heat is absorbed by water vapor in the plenum. The performance of a slurry-fed ceramic melter is quite different from the glass industry rule of thumb given above.

THEORETICAL/NUMERICAL MODELS

A basic understanding of the phenomenon affecting melter performance is important for melter design. The melter tank environment can be described by a set of differential equations relating the glass properties, fluid dynamics, and boundary conditions. Several investigators have modeled the melter tank region using two- and three-dimensional numerical simulations of the fluid dynamics and boundary conditions. In many cases, the computer-generated simulations were validated using physical model data.

Hjelm and Donovan (1979) used a two-dimensional computer code (VECTRA) to simulate an LFCM during idling and feeding modes. For the liquid feeding mode, the cold cap was assumed to be a 2-in. (5-cm) crust that had a thermal conductivity of 0.05 Btu/h-ft-°F (0.9 w/m-°C) based on the measured value for glass at 700°C. It was assumed that a 0.5-in. (1.3-cm) boiling liquid layer at 150°C was located above the cold cap. To account for endothermic reactions that take place in the crust, a heat sink of -2 kW was applied. The boundary

conditions were an ambient temperature of 27°C and a cooling jacket temperature of 38°C. The model was run until the heat transfer out of the system equaled the power input. The controlling parameter was the electrode temperature of 1050°C.

The results of the simulation showed that the corners of the melter tank and the entire tank floor were cooler in the idling mode. The fluid flow velocities were three times greater for the feeding mode, which causes more mixing and less temperature stratification between the top and the bottom of the glass. The temperatures computed in the floor refractory were higher than those measured in the actual LFCM because the model is two-dimensional and ignores heat transport perpendicular to the plane modeled.

A more comprehensive three-dimensional computer code (TEMPEST) was developed for modeling heat transfer in glass (Trent, Eyler, and Budden 1983). The TEMPEST computer code was verified using small-scale and physical model results for a dual electrode configuration. Limited comparisons were also made with actual PNL pilot-scale ceramic melter (PSCM) operating data.

Melter simulation results indicate that a dual electrode pair gives better mixing control than a single electrode pair and that the best power configuration is an equal split between the upper and lower electrodes. The TEMPEST results also show that large time-dependent temperature variations occur in the central regions of the glass melt caused by heat transfer to the cold cap. Comparisons between TEMPEST predictions and PSCM results, however, are inconclusive because insufficient physical property and boundary condition measurements are available. Further model development is needed to ensure that thermal equilibrium is attained and to improve the thermal radiation modeling at the cold cap (Eyler et al. 1985).

PHYSICAL MODELS

Physical models have also been tested to gain a better understanding of melter performance. Results of the physical modeling work have been used for numerical model validation and give further insight into the factors affecting scale-up and processing rate.

Several investigators have studied melter tank fluid dynamics using a scale model in which dimensionless similarity parameters were developed from simplification of the differential equations describing heat and mass transfer. A lithium-chloride-glycerine mixture was used to simulate both the fluid kinematic viscosity and the electrical resistivity in small plexiglass models. Boundary temperatures at the walls and at the simulated cold cap were maintained with cooling jackets.

Cold modeling by Quigley and Kreid (1979) on a one-third-scale model measured fluid velocities from 0.1 to 0.6 mm/s and showed two large counter-rotating cells. Inside the cells, flow was well-mixed. Using "streak photography," the results showed that simple plate electrodes gave a circulation pattern down the face of the electrodes and up in the center of the glass tank. The flow was nearly laminar at the bottom of the melter tank, and temperatures were cooler than in the center of the tank. Dual electrode bar pairs at a 1:1 power ratio gave better mixing and a warmer floor than a single electrode pair.

Robinson et al. (1984) modeled this same mixing pattern with a plug-flow region (20% of melt volume) and a well-mixed region (80% of melt volume). Flow patterns were measured using dye injection and time-lapse photography. Simulated idling conditions produced a circulation loop in front of the electrodes and at either end of the nonelectrode walls. Simulated feeding conditions also gave a circulation pattern under the cold cap, indicating that good mixing probably occurred close to the cold cap interface.

Routt (1982) modeled a one-half-scale cylindrical melter. He found the highest velocities in the gap between the electrode and the wall (<1 mm/s) and the lowest on the floor (0.02 mm/s). Velocity measurements were made by illuminating -100 mesh anthracene particles with a collimated light source and then photographing the particles. Electrical parameters predicted by the model were similar to actual melter values. Temperature profiles were more skewed in the model than in the actual melter, but differences may be due to a lower viscosity glass composition than modeled.

Although both the physical modeling and the numerical simulations reported here give insight into melter performance, neither addresses the major design

considerations of processing rate and cold cap performance because both are based on a static system. Neither approach considers inflow and outflow of material. In addition, the cold cap is considered a boundary condition without regard to its dynamic behavior, e.g., changing thickness and area. The physical and numerical models, however, do provide velocity data that are important for determining heat transfer to the cold cap and hence the melt rate.

COLD CAP HEAT TRANSFER MODEL

Routt and Porter (1980) modeled the cold cap using mass balance, heat transfer equations, and buoyancy of the cold cap. In the model, the cold cap consisted of three parts: 1) boiling slurry, 2) crust above the melt, and 3) crust below the melt. Six equations were solved for the height and mass flux of each layer. The maximum feed rate of a melter was predicted from heat transfer constraints using certain assumptions for radiant and convective heat transfer in the plenum. Heat of reaction in the feed pile (cold cap) was ignored. Theoretical calculations were compared with data from a PNL pilot-scale melter experiment conducted in September 1980. The predicted slurry feed rate was within 20% of the measured slurry feed rate.

Routt's model indicates that the radiant heat transferred from the walls and lid to the cold cap exceeds the heat transferred from the melt to the cold cap for wall temperatures over 600°C. The shape and size of the cold cap become more important with radiant heat transfer since the diameter and height of the cold cap above the melt determine the radiant heat transfer area. The model predicts that for a small-diameter cold cap the thickness decreases with wall temperature. For larger diameter cold caps, the thickness increases with wall temperature. This implies that different mechanisms control the melt rate as melter size changes.

Heat transfer between the bottom of the cold cap and the bulk glass was calculated using boundary-layer theory, although no computational details were given by Routt. Boundary-layer theory suggests that heat transfer from a surface to a fluid can be approximated by conductive heat transfer through a stagnant, finite layer of fluid (Bird, Stewart, and Lightfoot 1960). The entire temperature drop or rise takes place across this layer. The boundary-

layer thickness is calculated as a function of the Prandl number and an assumed fluid velocity profile, although Routt gives no calculational details.

Routt's (Routt and Porter 1980) cold cap model is potentially useful for scale-up calculations. Although PNL experiments using lid heaters (experiment numbers PSCM-4 and PSCM-5) did not confirm the predicted strong effects of plenum temperatures on rates, the Routt model may provide input to a scale-up model that integrates processing rates, cold cap behavior, and melter tank dynamics.

EXPERIMENTAL WORK

Experimental work conducted in five different-scale liquid-fed ceramic melters (LFCMs) is included in the scope of this scale-up study. These melters are the pilot-scale ceramic melter (PSCM), high-bay ceramic melter (HBCM), experimental ceramic melter (ECM), and liquid-fed mini-melter (LFMM) at the Pacific Northwest Laboratory (PNL), and the large slurry-fed melter (LSFM) at the Savannah River Laboratory (SRL). Table 1 summarizes their important characteristics, and a description of the major features of each of these melters is included in Appendix A.

Data from previous melter experiments were examined to select experiments that were run in melters of different scale but conducted under the same operating conditions. Processing rate data from these experiments were then compared to determine factors of scale. Two different melter feed compositions were selected for study: a SRL waste composition (SRL-TDSF-131) and a Hanford Waste Vitrification Plant (HWVP) composition (HW-39). The compositions of these simulated waste streams are given in Appendix A. Because neither composition had been run in all of the available melters, additional experiments were conducted to fill the gaps in the experimental data base. Details of the melter experiments included in the scope of this study are given in Appendix A, and a summary of the experimental data is given in Table 2.

The nominal and maximum feed rates from the melter runs in the experimental matrix were compared with those predicted by theoretical models of melter

TABLE 1. Melter Characteristics

Characteristic	LSFM	PSCM	HBCM	ECM	LFMM
Surface Area, m^2	1.1	0.73	0.25	0.054	0.0029
Glass Oepth, cm	61	42	22	15	10.6
Glass Volume, L	670	290	50	8.2	0.3
Design Throughput, 350 g oxide/L feed:					
Nominal Feed Rate, L/h	66	44	15	3	0.1
Maximum Feed Rate, L/h	88	58	20	4	0.2

TABLE 2. Summary of Experimental Data

	SRL-TDSF-131 Feed				HWVP Feed with Sugar				HWVP Feed Without Sugar			
Feed	PSCM4	HBCM861	LFMM861	LSFM9	PSCM22A	HBCM851	ECM861A	LFMM862	PSCM22B	HBCM862	ECM861B	LFMM863
Total Run Time, h	107.3	93	13	1,512	427	71.5	52.7	14	427	149	52.7	12
On-Line Efficiency, %	100	89	95	98.1	98.8	91	91	95	98.8	97.6	91	95
Nominal Feed Rate, L/h	57.3	14.2	0.43	85.3	36.9	11	2.2	0.29	42.8	17.3	2.9	0.35
Maximum Feed Rate, L/h	62	15.5	0.55	--	40.9	13.7	--	0.34	52.5	18.9	3.3	0.49
Feed Processed, L	6,150	1,147	6.02		5,995	1,095	58	4.94	8,426	2,242	64	5.19
Glass Produced, kg	2,709	592	2.66	65,000		390		1.69		1,090	48.4	1.14
Glass Temperature, °C	1,150	1,132	1,063	1,150	1,170	1,170	1,120	1,070	1,150	1,155	1,100	1,063
Cold Cap Temp., °C	850	958	1,013	850	950	798	820	1,020	880	908	770	1,013
Plenum Temperature, °C	600	542	1,003	800	300	494	670	1,010	280	440	630	1,003
Feed Density, kg/L	1.3	1.3	1.3	1.35	1.23	1.31	1.27	1.27	1.23	1.29	1.18	1.18

performance. The nominal feed rate is defined as the rate that can be maintained for an indefinite period of time while all operational parameters fall within accepted ranges. A maximum feed rate pushes the system to the limit; one or more of the standard operating parameters are on the verge of being exceeded. Feed surges may then lead to instability because minimal excess capacity remains. At the nominal rate, the cold cap coverage is approximately 80% with good venting and flexibility. At the maximum rate, the cold cap coverage is approaching 100%. The experimental determination of nominal and maximum feed rates is fairly subjective and introduces uncertainty in the scale-up analysis.

CORRELATION OF RESULTS

One of the most fundamental aspects of melter scale-up is determining the processing rate and maximum operating capacity. While the numerical and physical models developed for melters predict process conditions within the melter (such as temperature and circulation velocity), they are not yet capable of predicting melt rate for even steady-state conditions. The cold cap heat transfer model developed by Routt (1983) is an attempt to predict melt rate by analyzing the conditions which exist at the slurry-melt interface. Slurry feed rates and glass melt rates for five LFCMs were correlated using the melter surface area and the Routt heat transfer model. Comparison of the Routt model calculations with simple rate-to-surface area correlations indicates that the model is not sophisticated enough to improve upon melter surface area scale-up predictions.

SCALE-UP BY MELTER SURFACE AREA

The traditional method for LFCM scale-up is by melter surface area. Because the heat transfer to the cold cap from the bulk glass is via conduction, this approach seems reasonable and is generally supported by the data as a first approximation. Figures 1 and 2 show the nominal slurry feed rate

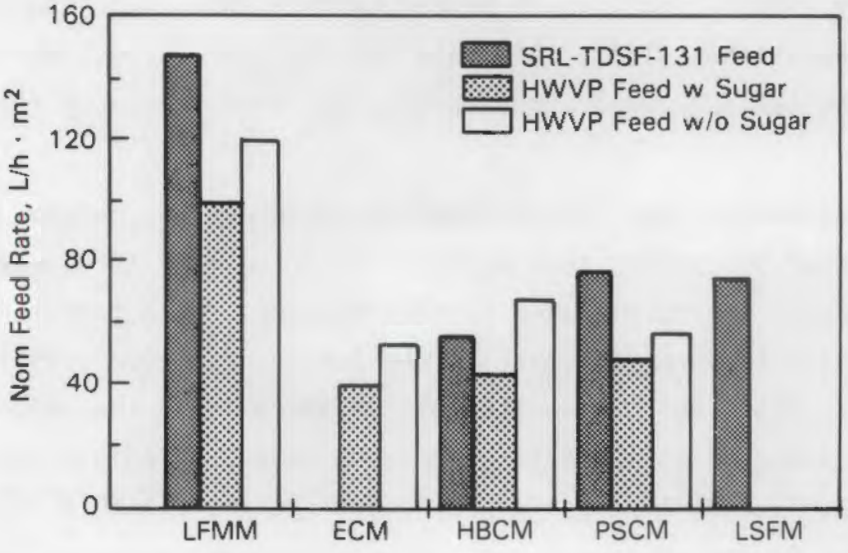

FIGURE 1. Nominal Slurry Feed Rate (feed rate/surface area)

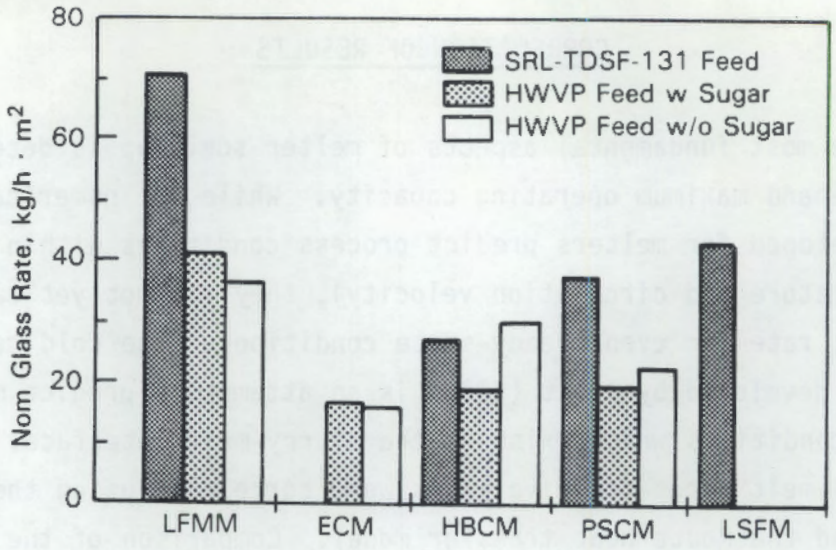

FIGURE 2. Nominal Glass Melt Rate (melt rate/surface area)

and the nominal glass production rate divided by the melter surface area for the experiments studied. The melter data are plotted in order of increasing size from the LFMM (surface area = 0.0029 m^2) to the LSFM (surface area = 1.12 m^2). The calculations are shown in Table 3. The correlation between surface area and feed rate is fairly good for the four largest melters. The nominal feed rates for these melters are within 20% of each other for the same glass composition. As indicated by Figures 3 and 4, the slurry feed rate and melt rate are nearly linear functions of melter surface area. For the SRL feed composition, the average slurry feed rate for the four largest melters was 71 L/h-m^2. For the two HWVP feed compositions, the average slurry feed rate was 53 L/h-m^2.

The data generated from the mini-melter, which is now under development, show a much higher throughput than would be expected from the larger melter data. Edge effects may have caused this difference. Heat transfer to the cold cap from the walls is more important in the 2.5-in. diameter vessel than in larger melters. Also, the mini-melter plenum space is in the heated zone, which would be expected to increase processing rates by radiant heat transfer to the cold cap. The mini-melter aspect ratio (height/$\sqrt{\text{width x length}}$) is much larger than that in the other melters. Circulation patterns and heat transfer may be impacted.

TABLE 3. Melter Scale-Up Calculations

Melter Characteristics	LFMM	ECM	HBCM	PSCM	LSFM
Surface Area, m^2	0.0029	0.054	0.25	0.73	1.12
Glass Volume, L	0.3	8.2	50	290	680
Glass Depth, cm	10.6	15.2	22	42	61
Aspect Ratio, $h/\sqrt{wxl}$	1.97	0.65	0.44	0.49	0.58
SRL-TDSF-131 Feed					
Run Number	LFMM-86-1	No	HBCM-86-1	PSCM-4	LSFM-9
Cold Cap Cover, %	80	Data	80	80	50
Nominal Feed Rate, L/h	0.43	Available	14.2	57.3	85.3
Slurry Feed Flux Rate, $L/h \cdot m^2$	148.28		56.80	78.49	76.16
Glass Flux, $kg/h \cdot m^2$	71.32		27.32	37.76	43.18
Fraction Solids in Feed	0.37		0.37	0.37	0.42
Feed Density, g/cm^3	1.3		1.3	1.3	1.35
Melt Rate, kg/h	0.21		6.83	27.56	48.37
Nom. Res. Time, h	1.45		7.32	10.52	14.06
HW-39 Feed With Sugar					
Run Number	LFMM-86-2	ECM-86-1A	HBCM-85-1	PSCM-22	
Cold Cap Cover, %	80	80	80	80	No
Nominal Feed Rate, L/h	0.29	2.2	11	36.9	Data
Slurry Feed Flux Rate, $L/h \cdot m^2$	100.00	40.74	44.00	50.55	Avail-
Glass Flux, $kg/h \cdot m^2$	41.91	17.07	19.60	19.90	able
Fraction Solids in Feed	0.33	0.33	0.34	0.32	
Feed Density, g/cm^3	1.27	1.27	1.31	1.23	
Melt Rate, kg/r	0.12	0.92	4.90	14.52	
Nom. Res. Time, h	2.47	8.89	10.21	19.97	
HW-39 Feed Without Sugar					
Run Number	LFMM-86-3	ECM-86-1B	HBCM-86-2	PSCM-22	
Cold Cap Cover, %	80	80	80	80	No
Nominal Feed Rate, L/h	0.35	2.9	17.3	42.8	Data
Slurry Feed Flux Rate, $L/h \cdot m^2$	120.69	53.70	69.20	58.63	Avail-
Glass Flux, $kg/h \cdot m^2$	37.03	16.48	30.35	23.08	able
Fraction Solids in Feed	0.26	0.26	0.34	0.32	
Feed Density, g/cm^3	1.18	1.18	1.29	1.23	
Melt Rate, kg/h	0.11	0.89	7.59	16.85	
Nom. Res. Time, h	2.79	9.22	6.59	17.21	

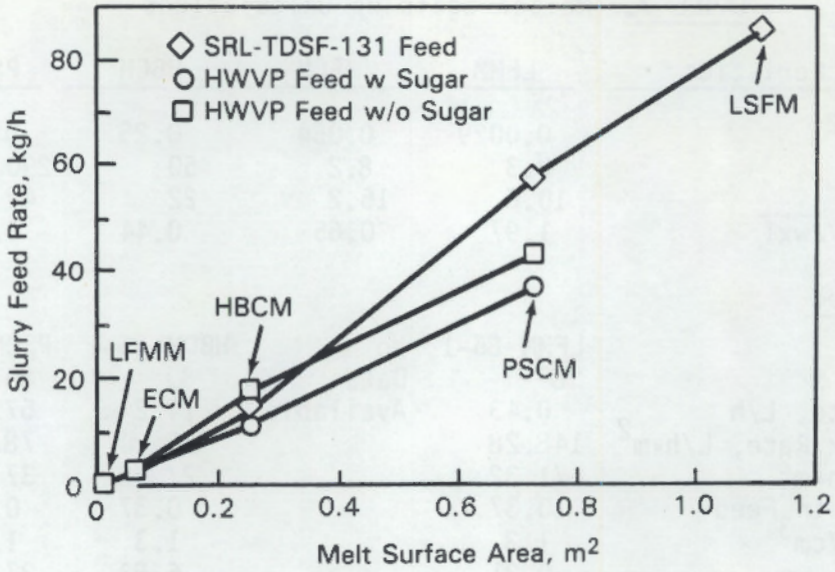

FIGURE 3. Feed Rate Versus Surface Area

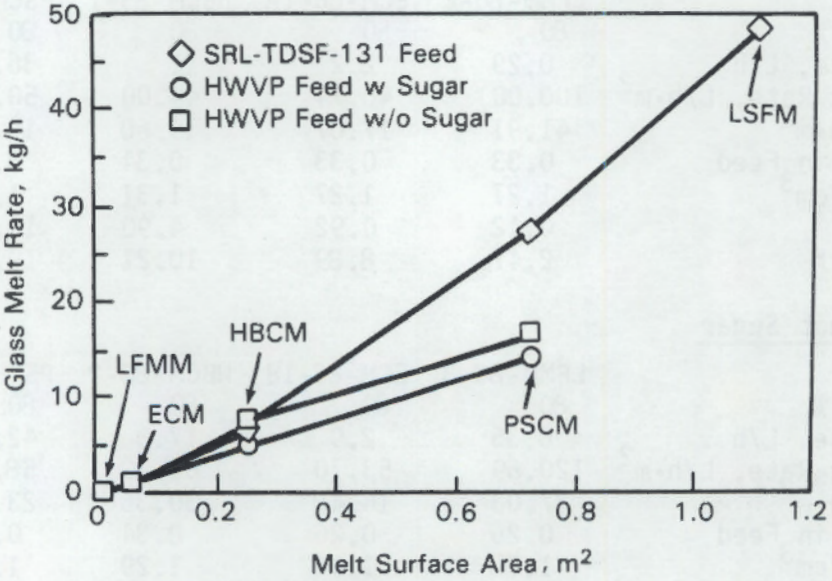

FIGURE 4. Melt Rate Versus Surface Area

SCALE-UP BY COLD CAP HEAT TRANSFER

Glass melt rates were calculated using the heat transfer model developed by Routt and Porter (1980) for each melter experiment studied. Appendix B gives the melter cold cap and glass data that were used in these

calculations. Glass and plenum temperatures were available from run summaries, but much of the other data was estimated (as noted in Appendix B). The data for cold cap properties and temperatures were not available in most cases. Therefore, Routt's original estimates were used for the cold cap parameters.

A comparison of actual and predicted glass melt rates indicates that the Routt heat transfer model is not capable of accurately predicting melter processing rates, although some of the imprecision may be due to the lack of accurate input parameters. Figures 5, 6, and 7 show actual versus calculated glass melt rates (glass melt rate/surface area) for the SRL and two HWVP feed compositions. The glass melt rates calculated by the Routt heat transfer model are a factor of 2 to 14 lower than the actual rates. The predicted rates are based on boundary layer thicknesses calculated using a bulk glass velocity of 0.25 cm/s (Eyler et al. 1985). The calculated rate is sensitive to the boundary layer thickness computation. If a 0.025-m (1-in.) boundary layer thickness is used in the rate calculations, as Routt did for the PSCM (Routt 1983), the calculated melt rates, except for the mini-melter, are within 25% of the actual rates. (See Figures 8, 9, and 10.) However, Routt gives no boundary layer calculation details and a boundary layer thickness of 0.025 m would require a bulk glass velocity of 10 cm/s, well above the velocity possible without forced convection.

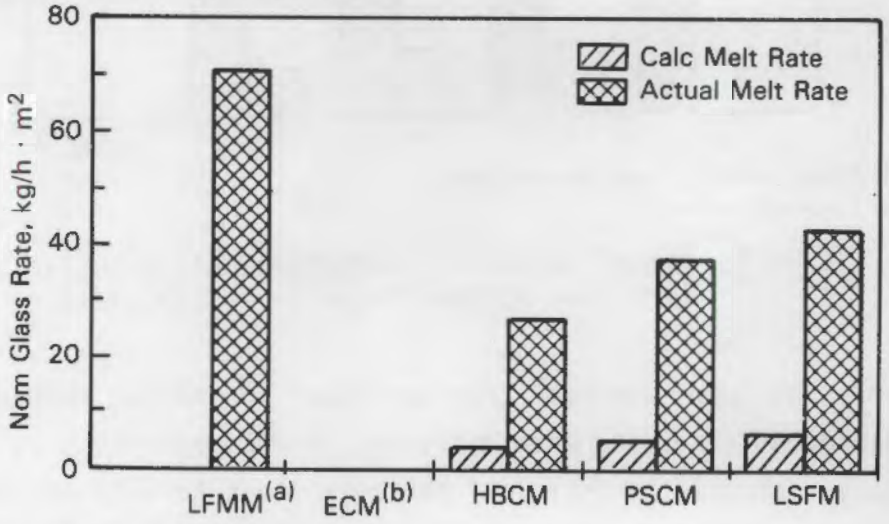

(a) Model predicts negative melt rate.
(b) Data not available.

FIGURE 5. Actual and Calculated Glass Melt Rate for SRL-TDSF-131 Feed (V = 0.25 cm/s)

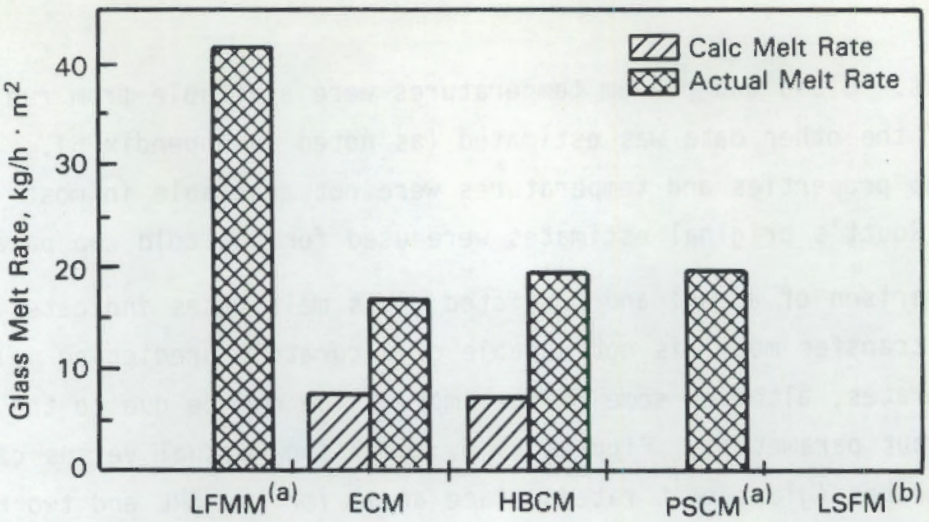

(a) Model predicts negative melt rate.
(b) Data not available.

FIGURE 6. Actual and Calculated Glass Melt Rate for HWVP Feed with Sugar (V = 0.25 cm/s)

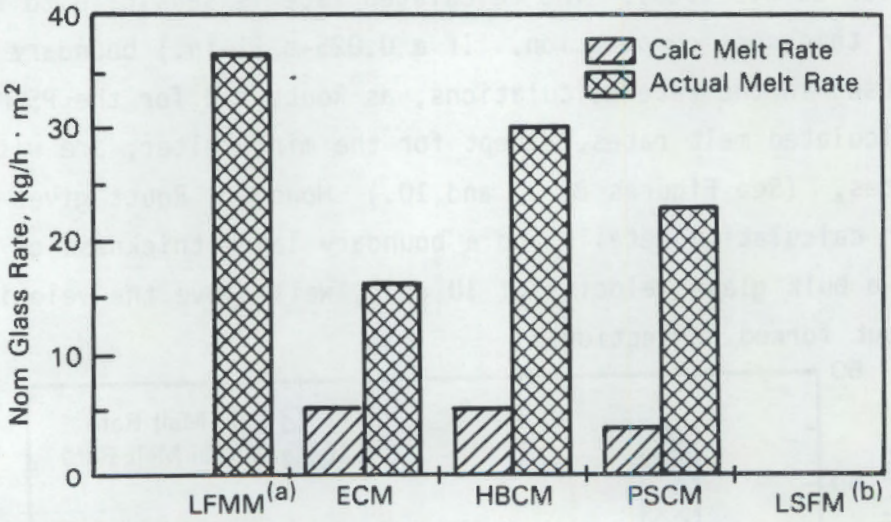

(a) Model predicts negative melt rate.
(b) Data not available.

FIGURE 7. Actual and Calculated Glass Melt Rate for HWVP Feed Without Sugar (V = 0.25 cm/s)

In its present form, the heat transfer model for melter scale-up between melters of different sizes and with different feed compositions is limited. Routt's model is potentially useful if the bulk glass to cold cap heat transfer calculation can be improved. The numerical and physical modeling work may provide some of the data required. Finally, better physical property measurements will be needed to validate the heat transfer model.

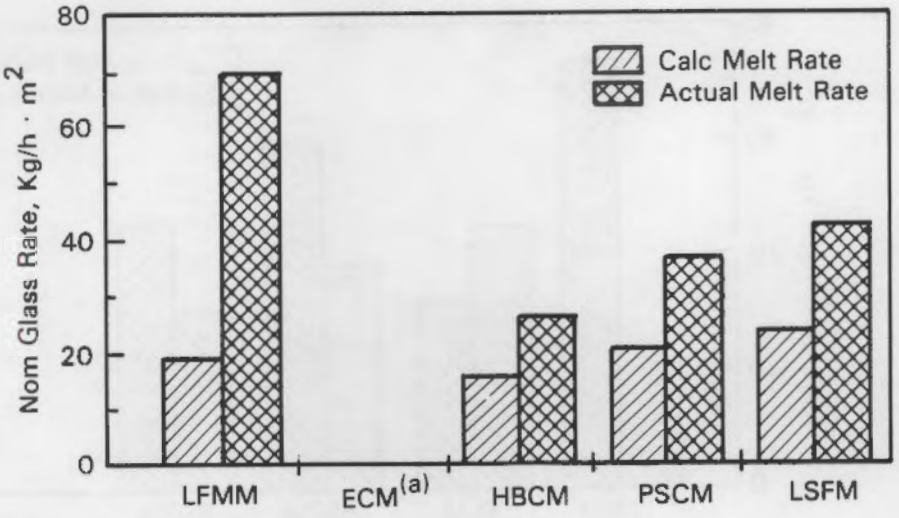

(a) Data not available.

FIGURE 8. Actual and Calculated Glass Melt Rate for SRL-TDSF-131 Feed (V = 10 cm/s)

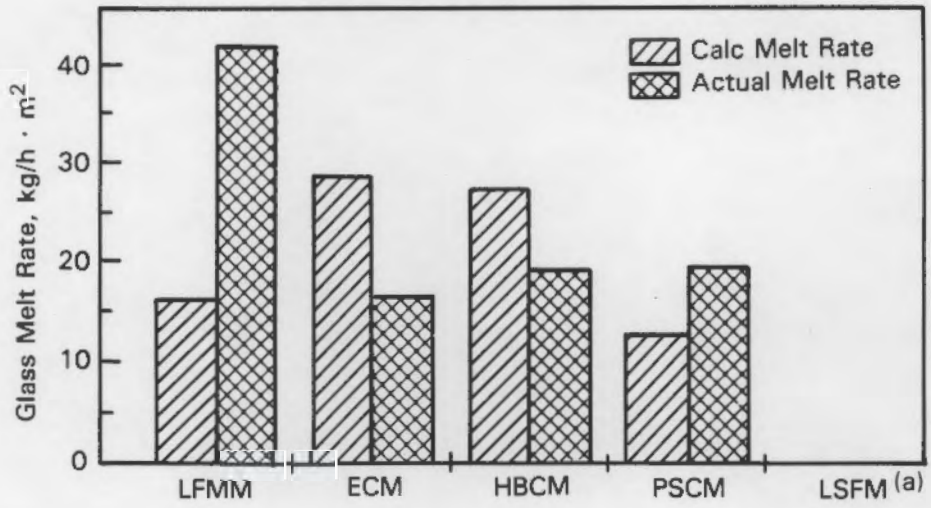

(a) Data not available.

FIGURE 9. Actual and Calculated Glass Melt Rate for HWVP Feed with Sugar (V = 10 cm/s)

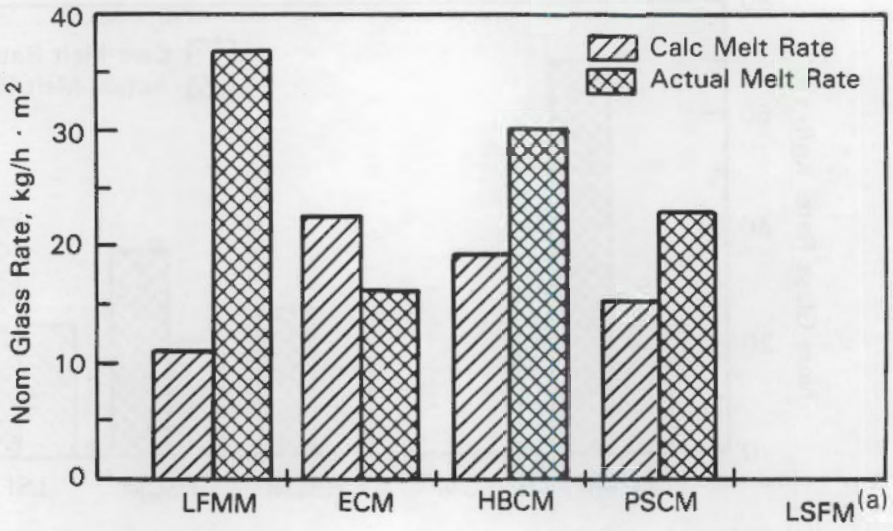

(a) Data not available.

FIGURE 10. Actual and Calculated Glass Melt Rate for HWVP Feed Without Sugar (V = 10 cm/s)

CONCLUSIONS AND RECOMMENDATIONS

The run summaries from ten LFCM experiments in five different-scale melters gave a broad range of melter performance data. The historical feed and temperature data were particularly useful in comparing melter processing capacities. Nominal melter feed rate divided by melter surface area gave a fair estimate of melter capacity and was reasonably independent of melter size. The average slurry feed rates for the four larger melters were 71 and 53 $L/h\text{-}m^2$ for the SRL and HWVP feeds respectively.

The mini-melter rate data did not follow the trends of the larger melters. The mini-melter had a much larger throughput than would be expected for its surface area. The discrepancy may have been caused by heat transfer to the cold cap directly from the heated plenum and walls as well as geometric differences.

A cold cap heat transfer model which takes into account glass and cold cap properties and melter physical parameters is a potentially useful method for predicting melter throughput capacity. However, the heat transfer model developed by Routt was not capable of accurately predicting melt rates for the ten LFCM experiments studied. In some cases the model actually predicted negative melt rates. Heat transfer at the glass-cold cap boundary was not adequately handled by boundary-layer theory in the model and some of the cold cap physical properties are difficult to measure so they were not normally collected during past experiments.

A heat transfer model such as the model developed by Routt should be further pursued as a scale-up tool. A reliable model which could calculate melter capacity based on laboratory physical property data would bridge the gap between small-scale bench experiments and large pilot- or demonstration-scale experiments. Measurements of cold cap temperature, thickness, and heat transport properties need to be made during melter operation to replace estimates with hard data and validate the model.

Additional work needs to be done to mesh the numerical and physical model melter information with a heat transfer model. Heat transfer at the glass-cold

cap interface requires additional study. Numerical simulations should give the fluid flow information necessary to improve or replace the boundary-layer heat transfer calculation.

An experiment should be designed to determine the relative effects of radiant heat transfer to the cold cap from above and convective heat transfer from the glass below on melt rate. Alternately, existing in-can melting data could be used to calculate radiant heat transfer parameters.

REFERENCES

Bird, R. B., W. E. Stewart, and E. N. Lightfoot. 1960. Transport Phenomena, p. 366. Department of Chemical Engineering, University of Wisconsin, John Wiley and Sons, Inc.

Bjorklund, W. J., and R. A. Brouns. 1983. "Dperating Characteristics of a Direct Liquid-Fed Vitrification Process." In Proceedings of the ANS Topical Meeting on the Treatment and Handling of Radioactive Waste, Battelle Press, Columbus, Ohio.

Bjorklund, W. J., et al. 1983. Savannah River Plant Defense Waste Vitrification Studies During FY 1982. PNL-4834, Pacific Northwest Laboratory, Richland, Washington.

Curran, R. L. 1971. "Use of Mathematical Modeling in Determining the Effect of Electrode Configuration on Currents in an Electric Glass Melter." IEEE Transactions on Industrial and General Applications, Vol. IGA-7 #1.

Eyler, L. L., et al. 1985. Physical and Numerical Modeling of Joule-Heated Melters. PNL-5491, Pacific Northwest Laboratory, Richland, Washington.

Hjelm, R. L., and T. E. Donovan. 1979. Numerical Modeling of Liquid Feeding in Liquid-Fed Ceramic Melter. PNL-3137, Pacific Northwest Laboratory, Richland, Washington.

Perez, J. M., Jr., and R. K. Nakaoka. 1986. Vitrification Testing of Simulated High-Level Radioactive Waste at Hanford. PNL-SA-13360, Pacific Northwest Laboratory, Richland, Washington.

Plodinec, M. J., et al. 1983. "SRP Radioactive Glass Studies: Small-Scale Process Development and Product Performance." In Proceedings of the ANS Topical Meeting on the Treatment and Handling of Radioactive Waste, Battelle Press, Columbus, Ohio.

Quigley, M. S., and D. K. Kreid. 1979. Physical Modeling of Joule-Heated Ceramic Glass Melters for HLW Immobilization. PNL-2809, Pacific Northwest Laboratory, Richland, Washington.

Reimus, M. A., S. C. Marschman, and G. L. Graff. 1986. Development of a Continuous Liquid-Fed Laboratory-Joule Mini-Melter for Nuclear Waste Glass Development. PNL-6073, Pacific Northwest Laboratory, Richland, Washington.

Robinson, K. S., et al. 1984. Development of Harwell Design JCM and First Trials of Third Scale Unit. UKDOE Report AERE-R 11082, AERE Harwell, Oxfordshire, England.

Routt, K. R. 1982. Physical Modeling of a Glass Melter Designed for Vitrification of Defense Waste. DP-MS-82-96, Savannah River Laboratory, Savannah River, Georgia.

Routt, K. R. 1983. "Theoretical Predictions for Continuous Slurry Feeding of a Glass Melter." Vol. 15 of Mat. Res. Soc. Symp. Proc., Elsevier Science Publishing Co., Inc.

Routt, K. R., and M. A. Porter. 1980. Theoretical Predictions for Continuous Glass Feeding of a Cylindrical Joule-Heated Melter. DPST-80-605, Technical Division, Savannah River Laboratory, Savannah River, Georgia.

Stanek, J. 1977. Electric Melting of Glass. Elsevier Science Publishing Co., Inc., New York.

Trent, D. S., L. L. Eyler, and M. J. Budden. 1983. Numerical Methods and Input Instructions. Vol. 1 of TEMPEST - A Three-Dimensional Time-Dependent Computer Program for Hydrothermal Analysis. PNL-4348, Pacific Northwest Laboratory, Richland, Washington.

Weisenburger, S. 1983. "High-Level Waste Vitrification Technique in a Full-Scale Pilot Plant." In Proceedings of the ANS Topical Meeting on the Treatment and Handling of Radioactive Waste, Battelle Press, Columbus, Ohio, pp. 190-196.

APPENDIX A

EXPERIMENTAL WORK DETAILS

APPENDIX A

EXPERIMENTAL WORK DETAILS

This section of the report contains the experimental work included in the scope of this scale-up study.

EXPERIMENTAL PLAN

Data from previous melter experiments were examined to select experiments that were run in melters of different scale but were conducted under the same operating conditions. Processing rate data from these experiments were then compared to determine factors of scale. Two different melter-feed compositions were selected for this study: a Savannah River Laboratory (SRL) composition (SRL-TDSF-131) and a Hanford Waste Vitrification Plant (HWVP) composition. Because neither composition had been run in all four of the available Pacific Northwest Laboratory (PNL) melters, experiments were conducted to fill gaps in the experimental data base. One experiment in a large-scale SRL melter was also included in the study.

The melter processing rates were compared using the nominal and maximum feed rates. The nominal feed rate is the rate that can be maintained for an indefinite period of time because all operational parameters (feed rate, plenum, and cold cap temperatures) fall within accepted ranges. A maximum feed rate pushes the system to the limit; one or more of the standard operating parameters are on the verge of being exceeded. Feed surges may then lead to instability because minimal excess capacity remains. At the nominal rate, the cold cap coverage was approximately 80% with good venting and flexibility. At the maximum rate, the cold cap coverage was approaching 100%.

MELTER DESCRIPTIONS

Five different liquid-fed ceramic melters (LFCMs) were included in the scope of this study. They are the pilot-scale ceramic melter (PSCM), high-bay

ceramic melter (HBCM), experimental ceramic melter (ECM), and liquid-fed mini-melter (LFMM) at PNL and the large slurry-fed melter (LSFM) at SRL. The following narrative describes the major features of each of these melters.

Pilot-Scale Ceramic Melter

The PSCM, PNL's largest operating nonradioactive melter, is a joule-heated, refractory-brick-lined melter with an exposed glass surface area of 0.73 m^3. During operating conditions, a glass depth of about 42 cm and a glass inventory of about 290 L are maintained in the melter. A schematic of the PSCM is shown in Figure A.1. The melter is heated by two plate electrodes.

Temperature feedback is used to control power to the melter and keep the bulk glass temperature at 1150°C. The glass temperature is monitored with a seven-thermocouple bundle inside a thermowell.

During operation, glass is periodically transferred from the melt tank to a receiving canister via a glass riser and overflow trough. Glass enters the riser through a port in the side wall of the melt tank at floor level. Glass discharge is assisted by an airlift lance in the riser that bubbles air into the glass. The difference in apparent density of the glass/air mixture compared with the glass in the melt tank causes the glass in the riser to move up the riser and into the pour trough. The glass flows down the pour trough and into the receiving canister.

High-Bay Ceramic Melter

The HBCM is a joule-heated, refractory-brick-lined glass furnace. The dimensions of the melt cavity, with respect to the nominal glass level, are 66.0 cm long by 40.6 cm wide by 22.9 cm deep. These measurements correspond to a glass capacity of approximately 50 L. The exposed glass surface area of the HBCM is 0.25 m^2. The melter drain and back walls slope from 40.6 cm apart at the glass level to 31.8 cm apart along the floor. A schematic of the HBCM is shown in Figure A.2. The glass temperature is monitored with a six-thermocouple bundle in an off-centered thermowell. Temperature feedback control is used during HBCM operations. Glass discharge is accomplished by a

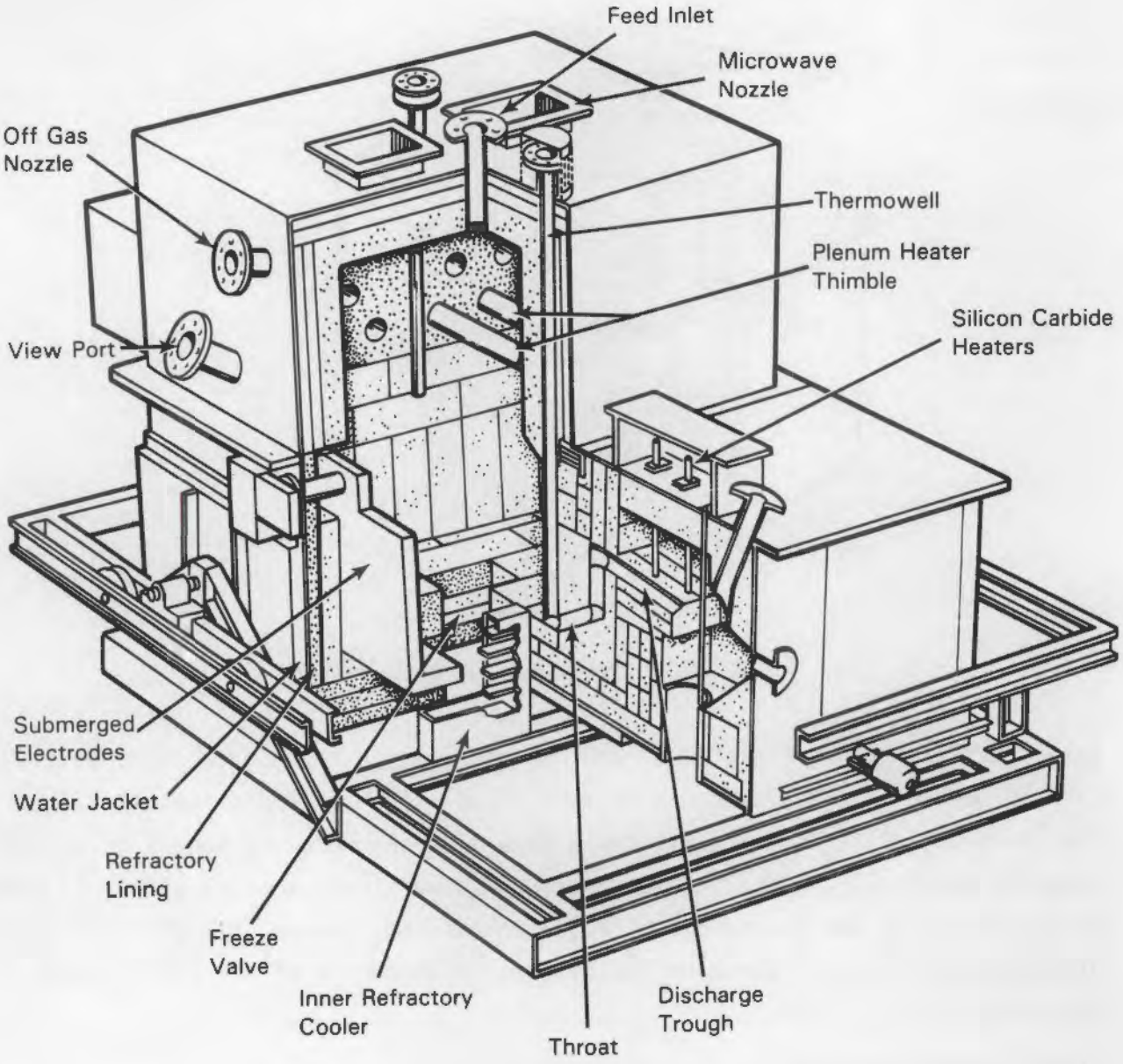

FIGURE A.1. Pilot-Scale Ceramic Melter

riser-overflow system with airlift assistance. However, the HBCM differs from the other PNL melters by having a sump and an associated sump electrode in the glass discharge section.

Experimental Ceramic Melter

The ECM is the smallest ceramic (joule-heated, refractory-brick-lined) melter at PNL and is used to perform preliminary scoping studies to evaluate

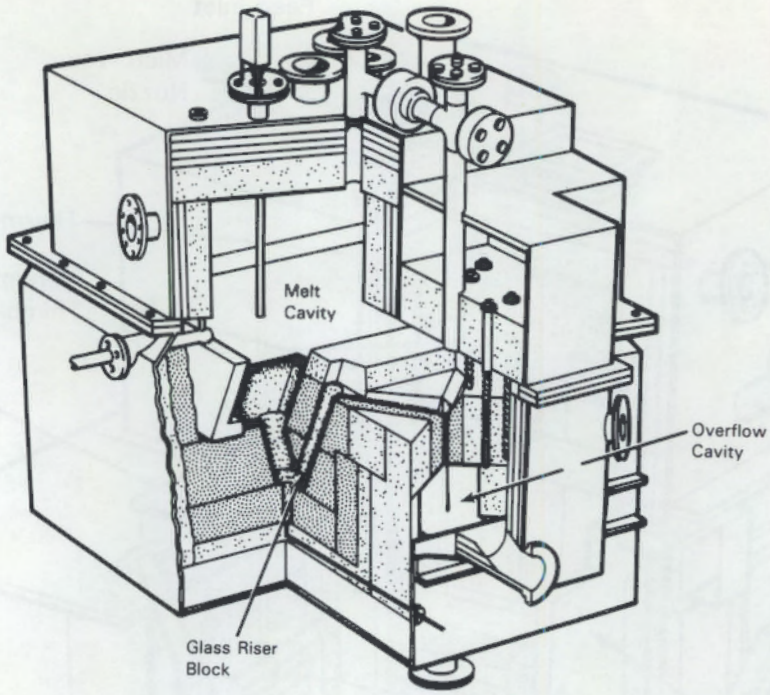

FIGURE A.2. High-Bay Ceramic Melter

feed processing characteristics. The exposed glass surface area is 0.054 m^2, and the operating glass depth is 15 cm. Glass volume is approximately 8.2 L. The glass temperatures are monitored with a five-thermocouple bundle in an off-centered thermowell. Under normal operating conditions, the glass melt is manually controlled and maintained at a bulk glass temperature of 1150°C. Glass discharges through a riser-overflow system. A schematic of the ECM is shown in Figure A.3.

Liquid-Fed Mini-Melter

The LFMM is a small laboratory-scale crucible melter designed for continuous operation (Reimus, Marschman, and Graff 1986). It is presently being developed as an experimental tool to simulate actual melter performance. The mini-melter consists of an Inconel crucible that is contained in a vertical tube furnace during operation. A glass-discharge tube is welded to the crucible side for good heat transfer and glass flow. A dam prevents the cold cap from entering the discharge section. The mini-melter crucible cavity has a

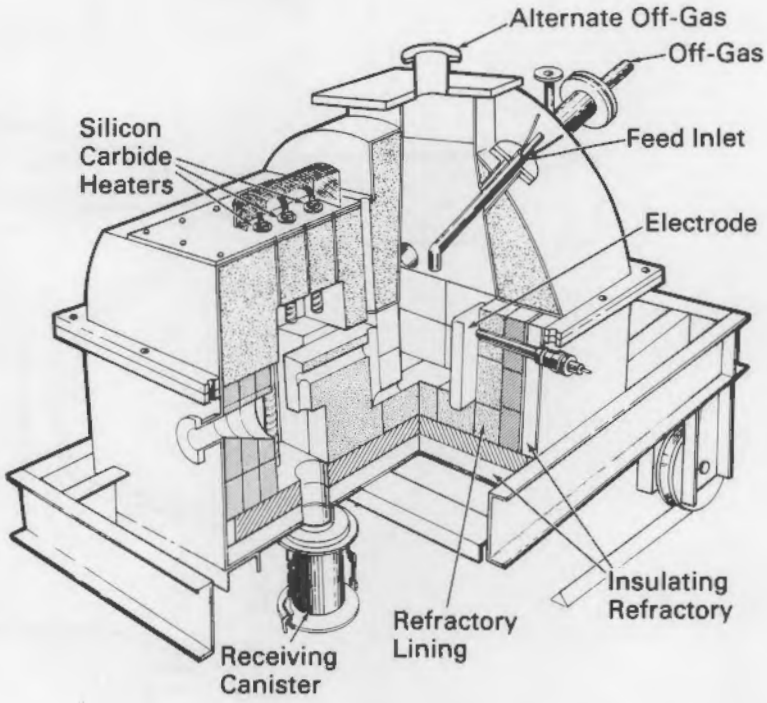

FIGURE A.3. Experimental Ceramic Melter

diameter of 6.4 cm (2.5 in.), a length of 16.5 cm (6.5 in.) and an exposed surface area of 0.0029 m^2 (4.5 $in.^2$). The operating glass depth is 10.6 cm, giving a glass volume of 300 mL. A schematic of the mini-melter is shown in Figure A.4. The glass temperature in the LFMM is monitored with a single thermocouple at the bottom of the crucible.

Large Slurry-Fed Melter

The LSFM is a large joule-heated, refractory-brick-lined melter at SRL. Four separate side-entering Inconel electrodes are spaced symmetrically around the octagonal tank. Melt pool heat is generated by firing ac current across the center of the tank between two electrode pairs. Twelve vertical silicon-carbide electrical-resistance heaters, located in the melter vapor space, supply the melter lid heat. The off-gas stream is drawn through the center of the lid. The feed nozzle is placed 28 cm (11 in.) off-center, which may cause

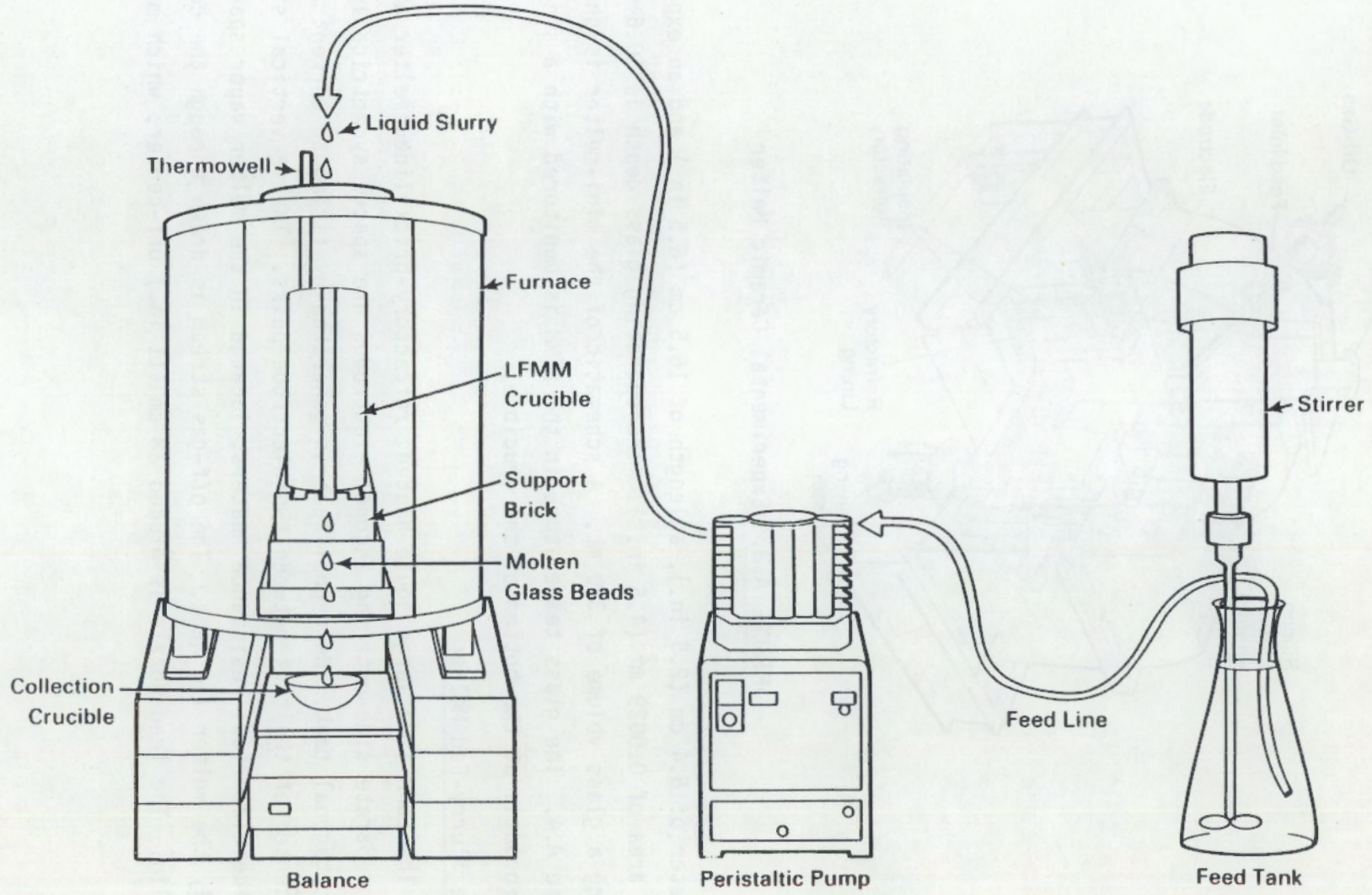

FIGURE A.4. Liquid-Fed Mini-Melter

uneven feed distribution on the melt surface and possibly a reduced melt rate. The melt surface area of the LSFM is 1.1 m^2 (12 ft^2), and the operating glass depth is 61 cm (24 in.). Schematics of the LSFM are shown in Figures A.5 and A.6.

EXPERIMENTAL RESULTS

Two different feed compositions, simulating high-level liquid waste streams from the Savannah River and Hanford Plants, were tested in the five melters discussed previously. A short summary of the experimental work included in the scope of this scale-up study follows, and Table A.1 shows the experiments performed.

Experiments with SRL Feed

PSCM-4

The PSCM-4 experiment was performed December 7 through 11, 1981. The major objective was to achieve the maximum feed rate without lid heating. The

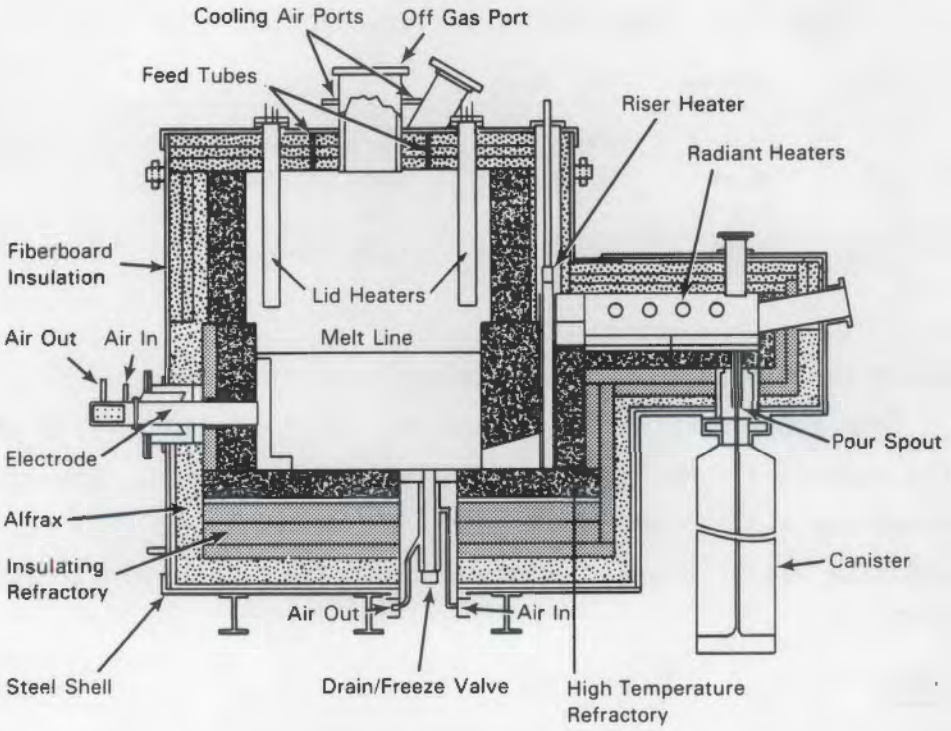

FIGURE A.5. Large Slurry-Fed Melter (side view)

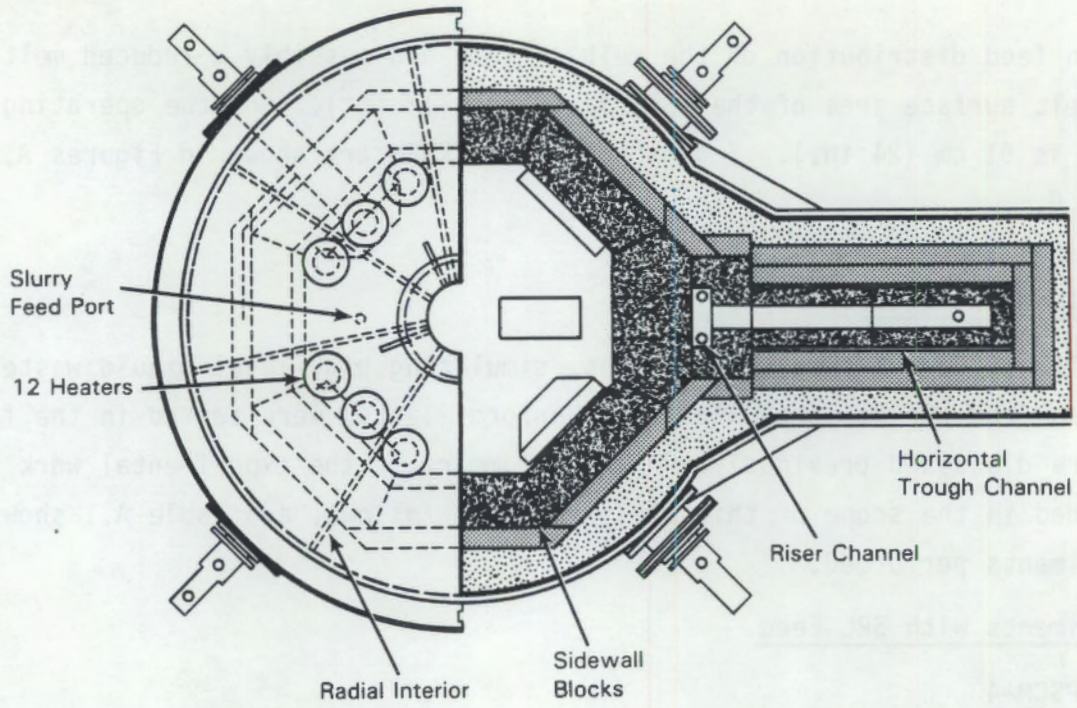

FIGURE A.6. Large Slurry-Fed Melter (LSFM) (top view)

TABLE A.1. Experiments Included in Scale-Up Study

Melter	SRL Feed	HWVP Feed
PSCM	PSCM-4	PSCM-22
HBCM	HBCM-86-1	HBCM-85-1 and 86-2
ECM		ECM-86-1
LFMM	LFMM-86-1	LFMM-86-2 and 3
LSFM	LSFM-9	

composition of the target feed (SRL-TDSF-131) for this experiment is given in Table A.2. This experiment was conducted for 107.3 h, and on-line efficiency was 100% (no downtime). No major problems were experienced. The amount of feed processed was 6150 L, and the total glass produced was 2709 kg. The average feed rate was 57.3 L/h, and the maximum feed rate maintained for over 26 h was 62.0 L/h.

HBCM-86-1

The HBCM-86-1 experiment was performed March 10 through 14, 1986, to fill gaps in an experimental matrix of data needed for this melter scale-up study.

TABLE A.2. SRL Simulated Waste Slurry and Glass Composition (SRL-TDSF-131)

Waste Slurry (2090 Liters)			Assumed Oxide Forms						
			Equivalent Weight, kg						
Compounds	Weight, kg	Conc., g/L	Oxide	TDSF Waste	(1) Frit-131	(2) Zeolite	Total	Final Glass Composition, wt%
Frit-131	713.4[a]	341.3						
Zeolite	20.7[b]	9.9						
$Fe(OH)_3$	169.8	81.2	Fe_2O_3	126.9			126.9	12.7
$Al(OH)_3$	71.4	34.2	Al_2O_3	46.7		4.0	50.7	5.1
$MnCO_3$	46.7[c]	22.3	MnO	28.8			28.8	2.9
$Mn(CHO_2)_2$	(58.9)	(28.2)						
$Ni(CO_2H)_2$	17.3	8.3	NiO	8.5			8.5	0.8
$Ca(CHO_2)_2$	35.0	16.7	CaO	15.1		2.2	17.3	1.7
SiO_2	32.6	15.6	SiO_2	32.6	413.0	9.9	455.5	45.6
$NaCHO_2$	17.6	8.42	Na_2O	8.0	126.3	0.5	136.3	13.6
$NaNO_3$	4.2	2.01		1.5				
Na_2SO_4	1.5	0.72	Na_2SO_4	1.5			1.5	0.1
$HCHO_2$	37.4	pH 5.5						
			B_2O_3		104.9		104.9	10.5
			Li_2O		40.6		40.6	4.1
			MgO		14.3		14.3	1.4
			TiO_2		7.1		7.1	0.7
			La_2O_3		3.6		3.6	0.4
			ZrO_2		3.6		3.6	0.4
Total	1142.4	546.6		269.6	713.4	16.6	999.6[d]	100.0

(a) Frit-131 Composition (-200 mesh)

Oxide	wt%
SiO_2	57.9
B_2O_3	14.7
Na_2O	17.7
Li_2O	5.7
MgO	2.0
TiO_2	1.0
La_2O_3	0.5
ZrO_2	0.5
	100.0

(b) Zeolite Composition (Linde Ionsiv IE-95)

Component	wt%
$CaAl_2Si_4O_{12}\ 6H_2O$	80
$Na_4Ca_{1.5}Al_3Si_8O_{24}\ 8H_2O$	20
	100

Assumed Oxide Forms	wt%
CaO	10.6
Al_2O_3	19.2
SiO_2	47.7
Na_2O	2.5
H_2O	20.0
	100.0

(c) Value based on reaction of $MnCO_3$ and $HCHO_2$.

(d) Feed slurry glass content = 0.478 kg/L.

The experiment was patterned after PSCM-4; operating temperatures and other operational parameters remained the same. Feed with the same target composition (SRL-TDSF-131), as shown in Table A.3, was prepared by the same procedures used during PSCM-4 feed makeup. During the experiment, a total of about 1147 L of feed was processed, producing a total of 592 kg of glass. An early problem with feed-line blockage due to agglomerated chemicals (resolved by installation of a strainer) resulted in an on-line efficiency of 89% for the 93-h test duration. The nominal feed rate was 14.2 L/h, and the maximum feed rate was 15.5 L/h.

LFMM-86-1

The LFMM-86-1 experiment was the first one performed in the developmental mini-melter and was run June 24 and 25, 1986. Feed left over from the HBCM-86-1 experiment was used with the same target composition as shown in Table A.3. The amount of feed processed during the 13-h experiment was 6.02 L, and the amount of glass produced was 2.66 kg. A nominal feed rate of 0.43 L/h and a maximum feed rate of 0.55 L/h were achieved. No major problems were experienced, and the feed behavior was similar to that exhibited in the larger melters.

LSFM-9

The LSFM-9 experiment was completed in the SRL melter on June 27, 1983, after 63 days of continuous operation. The primary objective was to demonstrate long-term, steady-state melter operation. The run progressed smoothly and achieved an on-line efficiency of 98.1%. Feed straining was required to eliminate most feed-line and feed-nozzle plugging. Nearly 72,000 kg of simulated waste glass were produced, filling 40 canisters at an average melt rate of 39.6 kg/h-m^2 (estimated feed rate of 85.3 L/h). No attempt was made to maximize melt rates during this run.

Melter operations included 39 days with frit-165 feed and 24 days with frit-131 feed. The results from the frit-131 feed will be used in the present study for comparison with the other runs made with frit-131 feed. The target composition used during this experiment is shown in Table A.3 and is very similar to the SRL-TDSF-131 feed (see Table A.2). For the feed rate used

TABLE A.3. LSFM-9 Feed Analysis

Component	Frit-165, wt%			Frit-131, wt%		
	Goal	ADD[(a)]	BR[(a)]	Goal	ADD[(a)]	BR[(a)]
$Fe(OH)_3$	13.2	15.9	12.2	13.2	16.4	12.9
$Mn(COOH)_2$	3.7	5.1	4.3	3.7	5.0	4.3
$Ca(COOH)_2$	2.5	3.5	3.3	2.5	4.1	3.0
$Ni(COOH)_2$	1.9	1.7	1.2	1.9	1.5	1.2
SiO_2	47.6	47.9	--	41.3	41.6	--
$Na_2O+NaNO_3+Na(COOH)$	12.5	11.6	11.5	15.9	14.4	15.4
$Al(OH)_3$	5.6	6.2	5.3	5.6	6.2	5.0
K(COOH)	0.2	0.3	0.6	0.2	--	0.6
Ce_2O_3	0.4	0.3	0.9	0.4	--	--
B_2O_3	6.2	6.4	4.5	9.0	9.7	8.0
Li_2O	4.3	4.7	3.5	3.4	3.6	3.0
MgO	0.6	0.6	0.4	1.2	1.1	0.8
ZrO_2	0.6	0.4	--	0.3	--	--
$CsNO_3$	0.09	0.08	0.02	0.09	0.06	0.03
$Sr(COOH)_2$	0.14	0.14	0.08	0.14	0.15	0.12
Na_2SO_4	0.22	0.24	0.18	0.22	0.15	0.27
$Ca_3(PO_4)_2$	0.15	0.29	0.1	0.15	0.27	--
$NaCl+CrCl_3$	0.05	0.15	0.11	0.05	--	0.08
CaF_2	0.05	0.14	0.01	0.05	--	0.04
TiO_2	--			0.4	0.5	0.2
La_2O_3	--			0.3	--	0.6
	100			100		

(a) Analysis from independent laboratories.

(85.3 L/h), the cold cap coverage was only 50%; and the cold cap was very thin (2 to 5 cm). Lid heating was applied to maintain an 800°C plenum temperature, which increased the feed processing rate.

Experiments with HWVP Feed

PSCM-22

The PSCM-22 experiment was completed on August 2, 1985, after 427 h of melter operation. Approximately 17,100 L of feed were processed, and 6,800 kg of glass were produced. The 18-day melter experiment was designed to evaluate the processing characteristics of the current HWVP melter feed (100% frit glass formers) on a pilot scale (Perez and Nakaoka 1986). The composition of the target feed for this experiment is shown in Table A.4.

TABLE A.4. Composition of HWVP Simulated Melter Feed Slurry[a,b]

Compound	Concentration, g/L	Assumed Oxide	Concentration, g/L	Glass, wt%
$Fe(OH)_3$	59.5	Fe_2O_3	44.4	11.10
$Al(OH)_3$	26.3	Al_2O_3	17.2	4.30
$NaHO_3$	13.4	Na_2O	10.7	2.68
$Cr(OH)_3$	7.21	Cr_2O_3	5.3	1.33
NaOH	3.58	ZrO_2	2.4	0.60
$Na_2C_2O_4$	3.37	SiO_2	3.0	0.75
$Zr(OH)_4$	3.11	NiO	2.4	0.60
SiO_2	3.00	SO_3	1.5	0.38
$Ni(OH)_2$	3.00	La_2O_3	2.2	0.55
Na_2SO_4	2.32	MoO_3	1.2	0.30
LaF_3	2.16	Nd_2O_3	2.1	0.53
$Na_2HoO_4\ 2H_2O$	2.00	Cs_2O	1.0	0.25
$Md(OH)_3$	1.84	CeO_2	0.7	0.18
CsOH	1.05	CuO	0.6	0.15
$Ce(OH)_3$	0.79	MnO_2	0.7	0.18
$Cu(OH)_2$	0.74	BaO	0.4	0.10
$Mn(OH)_2$	0.74	F^-	1.2	0.30
$BaSO_4$	0.63	SrO	0.4	0.10
NdF_3	0.58	Pr_6O_{11}	0.4	0.10
$Sr(OH)_2$	0.47	MgO	0.3	0.08
$Pr(OH)_3$	0.47	CaO	0.3	0.08
$La(OH)_3$	0.47	Y_2O_3	0.2	0.05
NaF	0.47	Sm_2O_3	0.02	0.05
$Mg(OH)_2$	0.42	TOC	0.6	0.05
CaF_2	0.42	I^-	0.04	0.01
$Y(OH)_3$	0.26			
$Sm(OH)_3$	0.21			
NaI	0.05			
Subtotals	138.56 g/L		99.4 g/L	24.9 wt%
HW39[d]	300.0	SiO_2	201.8	50.44
		B_2O_3	38.2	9.56
		Na_2O	30.8	7.69
		Li_2O	15.0	3.75
		CaO	11.2	2.81
		MgO	3.0	0.75
Subtotals	300.0 g/L		300.0 g/L	75.0 wt%
TOTALS	438.5 g/L		400.0 g/L	100 wt%

Reductants: 9.2 g/L formic acid, 3.5 to 0 g/L sugar.

(a) Basis: 400 g oxide/L slurry, 25 wt% waste oxide loading.
(b) Table does not currently show formated compounds.
(c) TOC substitute.
(d) HW39 frit size distribution as follows: 1/3 to be -80 -200 mesh, 2/3 to be -200 mesh.

One test objective was to investigate the effects of the redox level on stability of the glass melt and overall melter operation. Melter feed was processed with and without added reductant (sugar) during different segments of the test. The formatting process used in feed preparation added sufficient total organic carbon (TOC) to the melter feed to maintain a reducing feed without the addition of sugar. The redox potentials established during each segment of the run were sufficient to maintain stable processing.

No major problems were encountered during this experiment, and an on-line efficiency of 98.8% was achieved, excluding scheduled downtime. The feed without added reductant processed at higher rates than feed with added reductant. The nominal feed rates obtained were 36.9 L/h with added sugar (the reductant) and 42.8 L/h without sugar. The maximum feed rates obtained were 40.9 L/h with added sugar and 52.5 L/h without sugar.

HBCM-85-1

The HBCM-85-1 experiment was completed April 22, 1985, and consisted of five days of melter operation. During this experiment, two options for glass-former addition were tested (Perez and Nakaoka 1986). For the first three days of the run, the feed consisted of waste simulant and 100% of the glass formers added as frit. For the remaining two days, a feed was used in which the glass formers were added as 1/3 frit and 2/3 unreacted chemicals. The results of the feed-processability studies indicated that the 100% frit feed was superior in terms of feed rate and cold cap characteristics.

The results from the 100% frit case will be used in this melter scale-up study for comparison with other experiments using feed containing 100% of the glass formers as frit. The target feed composition for the HBCM-85-1 experiment was the same as that used for PSCM-22 and is shown in Table A.4. Sugar was added as a reductant during the HBCM-85-1 experiment. During the experiment, a total of 1095 L of feed was processed, and a total of 390 kg of glass was produced. The 100% frit portion of the run lasted 71.5 h, and an on-line efficiency of 91% was obtained. A nominal feed rate of 11.0 L/h and a maximum rate of 13.7 L/h were achieved during the 100% frit portion of the experiment.

HBCM-86-2

The HBCM-86-2 experiment began April 25 and was completed May 2, 1986. During the six-day test, a total of 2242 L of simulated melter feed was processed, producing over 1D90 kg of glass. The on-line efficiency for the 149-h test was 97%. This experiment was designed to evaluate the processing characteristics and to establish design and maximum feed rates for simulated melter feeds having total oxide (TO) concentrations greater than the FY 1985 reference value of 400 g TO/L. The HWVP experiment was the first to process the HWVP melter slurry containing all of the glass-forming frit in a single size range (-80/+200 mesh). The simulated waste feed had the same composition as that used in PSCM-22 (see Table A.4) except that sugar was not added as a reductant during this experiment. During the run, three different target TO concentrations were tested: 400 g TO/L, 500 g TO/L, and 650 g TO/L. The results of the 400 g TO/L case will be used by this melter scale-up study for comparison with other experiments that used the same oxide loading. The nominal feed rate for the HBCM-86-2 experiment with 400 g TO/L was determined to be 17.3 L/h, and the maximum feed rate was 18.9 L/h.

ECM-86-1

The ECM-86-1 experiment was performed May 21 through 23, 1986. This experiment was designed to allow data comparison with both PSCM-22 and HBCM-85-1. To make valid comparisons, the experimental constraints (including operating temperature and other operational variables) for PSCM-22 and HBCM-85-1 were imposed. Feed left over from the PSCM-22 experiment, which had aged for about one year, was used during the initial portion of this experiment, designated ECM-86-1A. However, this feed did not spread out over the surface of the melter; instead it formed volcano-like formations that built up to the feed nozzle. Because this problem appeared to be due to a change in the rheology of the feed during the one-year aging period, a decision was made to switch to feed from the HBCM-86-2 experiment, which was very similar in composition. Due to the feed problems encountered, the experiment had an overall on-line efficiency of 91%. The feed processed during the second portion of the experiment, designated ECM-86-1B, performed very well. This feed was left over from the recently completed HBCM-86-2 experiment and was very similar in

composition to the ECM-86-1A feed with the following exceptions: no sugar was added to this feed, and the frit was all the -80/+200 mesh size fraction.

During the 52.7 h duration of the ECM-86-1 experiment, 122 L of feed were processed--58 L of PSCM-22 feed during the initial portion, and 64 L of HBCM-86-2 feed during the second portion. A nominal feed rate of 2.9 L/h and a maximum feed rate of 3.3 L/h were determined for the HBCM-86-2 feed. A very approximate nominal feed rate of 2.2 L/h was determined for the aged PSCM-22 feed. Because of the processing problems encountered with this feed, this rate is not exact. A total of 48.4 kg of glass was produced during the course of this experiment.

LFMM-86-2

This experiment was conducted May 26 and 27, 1986, using the aged PSCM-22 feed containing sugar (as described in ECM-86-1A) to determine if the same poor feed-processing performance would be observed in the mini-melter. Similar volcano-like formations were observed. During the 14 h run, 4.94 L of feed were processed and 1.69 kg of glass were produced. The nominal feed rate determined was 0.29 L/h, and the maximum feed rate was 0.34 L/h.

LFMM-86-3

This experiment was conducted May 30 and June 1, 1986, using the HBCM-86-2 feed with 400 g TO/L and no sugar (for comparison with ECM-86-1B). During the 12-h run, 5.19 L of feed were processed, producing 1.14 kg of glass. A nominal feed rate of 0.35 L/h and a maximum feed rate of 0.49 L/h were obtained. This feed processed very well, duplicating the results obtained in ECM-86-1B.

APPENDIX B

ROUTT MODEL CALCULATIONS

TABLE B.1. Routt Model Calculations

		* * * SRL-TDSF-131 Feed * * *				* * * HWVP Feed w. Sugar * * *				* * * HWVP Feed w/o Sugar * * *			
Glass Properties		LFMM-86-1	HBCM-86-1	PSCM-4	LSFM-9	LFMM-86-2	ECM-86-1A	HBCM-85-1	PSCM-22	LFMM-86-3	ECM-86-1B	HBCM-86-2	PSCM-22
glass T cond (W/m-°C)	(1)	4.93	4.93	4.93	4.93	2.23	2.23	2.23	2.23	2.23	2.23	2.23	2.23
glass viscosity (poise)	(1)	8	8	8	8	80	80	80	80	80	80	80	80
glass temperature (°C)	(2)	1063	1132	1150	1150	1070	1120	1170	1170	1063	1100	1155	1150
crust bottom temperature (°C)	(2)	1013	958	850	850	1020	820	798	950	1013	770	908	880
boundry layer thickness (m)	(3)	0.079	0.167	0.200	0.215	0.037	0.060	0.078	0.093	0.037	0.060	0.078	0.093
heat of reaction (cal/g crust)	(4)	0	0	0	0	0	0	0	0	0	0	0	0
emissivity of wall	(4)	0.83	0.83	0.83	0.83	0.83	0.83	0.83	0.83	0.83	0.83	0.83	0.83
feed pile temperature (°C)	(4)	100	100	100	100	100	100	100	100	100	100	100	100
ABS feed pile temperature (°K)	(4)	373	373	373	373	373	373	373	373	373	373	373	373
spec heat - crust1 (cal/g-°C)	(4)	0.303	0.303	0.303	0.303	0.303	0.303	0.303	0.303	0.303	0.303	0.303	0.303
fraction solids in feed	(2)	0.37	0.37	0.37	0.42	0.33	0.33	0.34	0.32	0.26	0.26	0.34	0.32
offgas temperature (°C)	(2)	1003	542	500	800	1010	670	494	300	1003	630	440	280
steam enthalpy offgas(cal/g)	(4)	733.4	733.4	733.4	733.4	733.4	733.4	733.4	733.4	733.4	733.4	733.4	733.4
spec heat slurry (cal/g-°C)	(4)	0.6	0.6	0.6	0.6	0.6	0.6	0.6	0.6	0.6	0.6	0.6	0.6
slurry feed temperature (°C)	(4)	25	25	25	25	25	25	25	25	25	25	25	25
crust T cond (W/m-°C)	(4)	1.75	1.75	1.75	1.75	1.75	1.75	1.75	1.75	1.75	1.75	1.75	1.75
top of crust temperature (°C)	(4)	200	200	200	200	200	200	200	200	200	200	200	200
spec heat - crust2 (cal/g-°C)	(4)	0.2	0.2	0.2	0.2	0.2	0.2	0.2	0.2	0.2	0.2	0.2	0.2
feed density (g/cc)	(2)	1.3	1.3	1.3	1.35	1.27	1.27	1.31	1.23	1.18	1.18	1.29	1.23
crust density (g/cc)	(4)	1.329	1.329	1.329	1.306	1.405	1.405	1.645	1.203	1.210	1.210	1.476	1.203
glass density (g/cc)	(2)	2.11	2.11	2.11	2.11	2.17	2.17	2.17	2.17	2.17	2.17	2.17	2.17
side of crust temperature (°C)	(4)	463	463	463	463	463	463	463	463	463	463	463	463
ABS side/crust temperature (°K)	(4)	736	736	736	736	736	736	736	736	736	736	736	736
steam enthalpy crust (cal/g)	(4)	637	637	637	637	637	637	637	637	637	637	637	637
spec heat of glass (cal/g-°C)	(2)	0.369	0.369	0.369	0.369	0.35	0.35	0.35	0.35	0.35	0.35	0.35	0.35
wall temperature (°C)	(4)	368	368	368	368	368	368	368	368	368	368	368	368
ABS wall temperature (°K)	(4)	641	641	641	641	641	641	641	641	641	641	641	641
radius of feed pile (m)	(2)	0.024	0.226	0.386	0.486	0.024	0.105	0.226	0.386	0.024	0.105	0.226	0.386
melter surface area (m2)	(2)	0.0029	0.25	0.73	1.12	0.0029	0.054	0.25	0.73	0.0029	0.054	0.25	0.73
Other Constants		pi = 3.14159											
		sigma (S/B Constant) = 5.67 X 10-8											
Results													
feed pile height (m)		(5)	0.4369	0.1820	0.2299	(5)	0.0777	0.0858	(5)	(5)	0.0710	0.1660	0.2783
calc melt rate (kg/hr)		(5)	1.11	4.28	7.53	(5)	0.42	1.87	(5)	(5)	0.30	1.41	2.92
calc melt flux (kg/hr-m2)		(5)	4.43	5.87	6.72	(5)	7.82	7.49	(5)	(5)	5.61	5.63	3.99
actual melt flux (kg/hr-m2)		71.32	27.32	37.76	43.18	41.91	17.07	19.6	19.9	37.03	16.48	30.35	23.08

NOTES:

(1) Glass conductivity and viscosity data taken from SRL-TDSF-131 and PNL-5498.
(2) Data taken from experimental run summaries.
(3) See boundary layer calculations - Appendix C.
(4) From Routt's model DPST-80-605
(5) Model calulates a negative value

APPENDIX C

CALCULATION OF BOUNDARY-LAYER THICKNESS

APPENDIX C

CALCULATION OF BOUNDARY-LAYER THICKNESS

Calculation of the boundary layer thickness is included here to aid the reader in evaluating or modifying the Routt (1983) heat transfer model. As noted in the main text of the report, the heat transfer at the glass-cold cap interface is not sufficiently described by boundary layer theory. Melt rates were generally more than an order of magnitude higher than predicted by the Routt model, probably because the model grossly underpredicts heat transfer from the glass to the cold cap. An improved cold cap model may be possible using heat transfer data from the physical and numerical modeling data.

1. Assume the temperature and velocity profiles are the same shape and related by Δ (Bird, Stewart, and Lightfoot 1960).

2. Let δ = velocity boundary-layer thickness

   δ_T = temperature boundary-layer thickness ($\delta_T = \Delta \cdot \delta$)

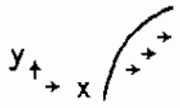

vx = velocity in x direction

$\eta = y/\delta$ = dimensionless depth (velocity profile)

$\eta_T = y/\delta_T$ = dimensionless depth (temperature profile)

$\phi = vx/v_\infty$ = dimensionless velocity

$$\Theta = \frac{T_0 - T}{T_0 - T_\infty} = \text{dimensionless temperature}$$

where T_0 = temperature at wall

T_∞ = bulk temperature

v_∞ = bulk velocity.

3. Assume parabolic temperature and velocity profiles.

$$\Theta = 2\eta_T - \eta_T^2 \qquad \phi = 2\eta - \eta^2$$

$$\Theta' = 2 - 2\eta_T \qquad \phi' = 2 - 2\eta$$

$$\Theta'' = -2 \qquad \phi'' = 2$$

4. For fluid flow past a slab, the Navier-Stokes equation is:

$$v_x \frac{\partial v_x}{\partial x} - \left(\int_0^y \frac{\partial v_x}{\partial x}\, dy\right) \frac{\partial v_x}{\partial y} = \nu \frac{\partial^2 v_x}{\partial y^2}$$

where ν = kinematic viscosity.

5. The energy equation is

$$v_x \frac{\partial T}{\partial x} - \left(\int_0^y \frac{\partial v_x}{\partial x}\, dy\right) \frac{\partial T}{\partial x} = \alpha \frac{\partial^2 T}{\partial y^2}$$

where α = thermal diffusivity.

6. When the dimensionless variables and the assumed velocity and temperature profiles are substituted, the equations can be solved for the boundary-layer thicknesses.

$$\delta = 5.477 \sqrt{\frac{\nu \chi}{v_\infty}}$$

$$\Delta = 0.928 \sqrt[3]{\alpha} = 0.928 \cdot P_r^{-1/3}$$

$$\delta_T = \delta \cdot \Delta$$

where χ = length of the slab

P_r = Prandtl number.

7. Calculation of δ_T

let $v_\infty = 0.25$ cm/s

$$\text{(Curran 1971)}\ v_\infty = 31\ \frac{ft}{h} = 0.26\ \frac{cm}{s}\ \text{for}$$

$$\text{(Eyler 1985)}\ v_\infty = 0.25\ \frac{cm}{s}$$

$$\Delta = 0.928\ \alpha^{1/3} = 0.928\ \left(\frac{k}{Cp\mu}\right)$$

where k = thermal conductivity [W/m • °C]

Cp = specific heat [cal/g • °C]

μ = viscosity [poise = g/cm • s]

$$\Delta = 0.928\ \left[\frac{k\ \left[\frac{w}{m \cdot c}\right]\ 8.6 \times 10^2\ \left[\frac{cal}{w \cdot h}\right]}{Cp\ \left[\frac{cal}{g \cdot {}^{o}C}\right]\ \mu\ \left[\frac{g}{cm \cdot s}\right]\ 3600\ \left[\frac{s}{h}\right]\ 100\ \left[\frac{cm}{m}\right]}\right]^{1/3}$$

$$\Delta = 0.124\ \left(\frac{k}{Cp\mu}\right)^{1/3}$$

let $\chi = R_f$ (radius of feed pile or cold cap)

$$\delta = 5.477\ \sqrt{\frac{\gamma\ \chi}{v_\infty}} = 5.477\ \sqrt{\frac{\mu \cdot R_f}{\rho \cdot v_\infty}}$$

where ρ = density [g/cc]

$$\delta = 5.477\ \sqrt{\frac{\mu\ \left[\frac{g}{cm \cdot s}\right]\ R_f\ [m]}{\rho\ \left[\frac{g}{cm^3}\right]\ 0.25\ \left[\frac{cm}{s}\right]\ 100\ \left[\frac{cm}{m}\right]}}$$

$$\delta = 1.095\ \sqrt{\frac{\mu R_f}{\rho}}\ [m]$$

$$\delta_T = \Delta\delta = 0.136\ \left(\frac{k}{Cp\mu}\right)^{1/3}\ \left(\frac{\mu R_f}{\rho}\right)^{1/2}$$

for SRL-131 feed

$$\delta_T = 0.136 \left(\frac{4.93}{0.369 \times 8}\right)^{1/3} \left(\frac{8 \times 0.386}{2.11}\right)^{1/2}$$

$$\delta_T = 0.195 \text{ m} = 7.7 \text{ inches}$$

DISTRIBUTION

No. of Copies

OFFSITE

10 DOE Office of Scientific and Technical Information Center

6 DOE Office of Civilian Radioactive Waste Management
Forrestal Building
Washington, DC 20585
ATTN: L. H. Barrett, RW-33
C. R. Cooley, RW-40
J. R. Hilley, RW-3D
S. H. Kale, RW-20
D. E. Shelor, RW-32
R. Stein, RW-23

4 DOE Office of Defense Waste & Transportation Management
GTN
Washington, DC 20545
ATTN: T. C. Chee, DP-123
K. A. Chacey, DP-123
G. H. Daly, DP-124
J. E. Lytle, DP-12

4 DOE Office of Remedial Action and Waste Technology
GTN
Washington, DC 20545
ATTN: J. A. Coleman, NE-24
T. W. McIntosh, NE-24
W. R. Voigt, NE-20
H. F. Walter, NE-24

A. T. Clark
Division of Fuel Material Safety
Nuclear Regulatory Commission
Washington, DC 20555

No. of Copies

V. Stello
Office of the Executive Director for Operations
Mail Station 6209
Nuclear Regulatory Commission
Washington, DC 20555

S. Meyers
Environmental Protection Agency
Office of Radiation Programs (ANR-458)
401 M Street S.W.
Washington, DC 2D460

J. M. McGough
DOE Albuquerque Operations Office
P.O. Box 5400
Albuquerque, NM 87185

P. G. Hagan
Joint Integration Office
Carlmont Executive 1
4308 Carlisle N.E.
Albuquerque, NM 87107

E. Maestas
DOE West Valley Project Office
P.O. Box 191
West Valley, NY 14171

3 DOE Idaho Operations Office
550 Second Street
Idaho Falls, ID 83401
ATTN: S. T. Hinschberger
J. P. Hamric
J. L. Lyle

F. T. Fong
DOE San Francisco Operations
1333 Broadway
Oakland, CA 94612

No. of Copies

M. R. Jugan
DOE Oak Ridge Operations Office
P.O. Box E
Oak Ridge, TN 37830

W. J. Brumley
DOE Savannah River Operations Office
P.O. Box A
Aiken, SC 29801

M. J. Steindler
Argonne National Laboratory
9700 South Cass Avenue
Argonne, IL 60439

C. S. Abrams
Argonne National Laboratory
P.O. Box 2528
Idaho Falls, ID 83401

3 Battelle Memorial Institute
Project Management Division
505 King Avenue
Columbus, OH 43201
ATTN: W. A. Carbeiner
W. S. Madia
Technical Library

L. D. Ramspott
Lawrence Livermore National Laboratory
University of California
P.O. Box 808
Livermore, CA 94550

D. T. Oakley, MS 619
Los Alamos Scientific Laboratory
P.O. Box 1663
Los Alamos, NM 87544

No. of Copies

4 Oak Ridge National Laboratory
P.O. Box Y
Oak Ridge, TN 37830
ATTN: J. O. Blomeke
W. D. Burch
R. T. Jubin
L. J. Mezga

Sandia Laboratories
P.O. Box 5800
Albuquerque, NM 87185
ATTN: R. W. Lynch
Technical Library

J. R. Berreth
Westinghouse Idaho Nuclear Co., Inc.
P.O. Box 4000
Idaho Falls, ID 83401

6 E. I. du Pont de Nemours Company
Savannah River Laboratory
Aiken, SC 29801
ATTN: R. G. Baxter
M. D. Boersma
J. G. Glasscock
J. R. Knight
M. J. Plodinec
C. T. Randall

E. A. Jennrich
EG&G Idaho
P.O. Box 1625
Idaho Falls, ID 83415

R. Shaw
Electric Power Research Institute
3412 Hillview Avenue
P.O. Box 10412
Palo Alto, CA 94304

No. of
Copies

3 West Valley Nuclear Services Company
P.O. Box 191
West Valley, NY 14171
ATTN: S. M. Barnes
R. A. Humphrey
J. M. Pope

J. L. White
Energy Research & Development Authority
Empire State Plaza
Albany, NY 12223

ONSITE

6 DOE Richland Operations Office

R. W. Brown, A5-53
C. E. Collantes, A6-50
M. J. Furman, A5-10
W. S. Ketola, A5-53
D. M. Smith, A6-90
J. J. Sutey, A5-90

7 Westinghouse Hanford Company

J. M. Henderson, B2-03
R. E. Lerch, R2-53
H. E. McGuire, R2-41
J. L. Scott, B2-03
D. D. Wodrich, R2-23
R. D. Wojtasek, R1-10
B. A. Wolfe, B2-04

No. of
Copies

40 Pacific Northwest Laboratory

C. R. Allen, B2-02
W. W. Ballard, Jr., K1-78
W. F. Bonner, P7-44
R. A. Brouns, P7-41
H. C. Burkholder, P7-41
T. T. Claudson, K1-45
M. R. Elmore, B2-02
R. W. Goles, B2-02
W. O. Heath, P7-41
S. S. Koegler (5), P7-18
W. L. Kuhn, P7-14
L. T. Lakey, A3-70
D. E. Larson, B2-02
J. L. McElroy, P7-18
S. J. Mitchell (5), P7-44
R. K. Nakaoka, P7-41
K. A. Parnell, P8-20
J. M. Perez, Jr., B2-02
M. E. Peterson, P7-44
M. A. Reimus, P7-14
W. A. Ross, P7-41
G. J. Sevigny, B2-02
D. H. Siemens, B2-02
S. C. Slate, P7-44
J. H. Westsik, Jr., P7-14
Publishing Coordination
Technical Report Filles (5)